



Photocatalytic degradation of methyl orange by Eu doped SnO₂ nanoparticles

T. T. Bhosale^{1,2} · A. R. Kuldeep¹ · S. J. Pawar³ · B. S. Shirke² · K. M. Garadkar¹

Received: 17 June 2019 / Accepted: 21 September 2019 / Published online: 28 September 2019
© Springer Science+Business Media, LLC, part of Springer Nature 2019

Abstract

An eco-friendly approach was adapted for the synthesis of Eu doped SnO₂ nanoparticles (NPs) by using aqueous leaf extract of *Calotropis gigantea*. The attempt was made to see the effect of Eu content in SnO₂ NPs on photocatalytic degradation of methyl orange (MO). The characterization of synthesized NPs was carried out by applying different techniques such as diffuse reflectance spectroscopy, fourier transform-infrared spectroscopy, X-ray powder diffraction (XRD), high resolution-transmission electron microscopy, field emission-scanning electron microscopy, energy dispersive X-ray analysis and photoluminescence spectroscopy. The XRD results confirmed, the polycrystalline nature and tetragonal rutile phase of Eu³⁺ doped SnO₂ NPs. Bandgap of pure SnO₂ is 3.1 eV which is reduced to 3 eV for 0.1 mol% Eu³⁺ hence doping is responsible for bandgap narrowing. Consequently, up to 90% photocatalytic degradation of MO by 0.1 mol% Eu³⁺ doped SnO₂ takes place within 3 h under UV–Vis light ($\lambda = 365$ nm). It is noted that doping of Eu enhances the efficiency of MO by 10%.

1 Introduction

Waste effluents from dye industries, tremendous use of pesticides and fertilizers in agricultural processes and their disposal led to increasing in the number of various organic pollutants in the natural water bodies. Most of these organic pollutants are non-biodegradable and by anaerobic degradation may produce carcinogenic intermediates [1]. Advanced oxidation process (AOP) using semiconductor photocatalyst is one of the best treatment for the industrial dye effluents [2].

In recent years, the research has been focused on the green synthesis methods for the production of metal oxide nanoparticles due to their novel, environmental friendly and

inexpensive approach [3, 4]. The metal oxide nanoparticles such as TiO₂ [5, 6], ZnO [7, 8] and SnO₂ [9] have been synthesized by green route, which are used as photocatalyst in the degradation of various dye pollutants. The semiconductor materials have attracted much more attention for photodegradation of the dye effluents from industries. Most of these semiconducting materials have wide bandgap hence they are capable to degrade the organic pollutant only in UV light. Additionally, by using large bandgap semiconductor as a photocatalyst, the rate of recombination of electron–hole pairs enhances which reduces the activity of photocatalytic reaction. All these difficulties can be overcome by doping the semiconductor with rare earth elements. A suitable dopant like rare earth elements creates quasi-stable energy states within the bandgap energy. Besides, doping of appropriate ions into the host lattice increases electron trapping owing to their higher surface sites and the difference in bandgap energy leads to an increase in photocatalytic activity [10]. Europium ion with 4f⁷ electronic configuration usually exist in the form of triply ionized ion (Eu³⁺), which shows fast oxygen ion mobility and predominant catalytic properties [11].

SnO₂ is a well-known wide bandgap (3.6 eV) n-type semiconductor which has been extensively used for various applications like gas sensors [12], transparent conducting electrodes [13], photocatalyst [14], Li-ion battery anode materials [15], dye-based solar cells [16] and optoelectronic

✉ B. S. Shirke
bss_chemistry@yahoo.com

✉ K. M. Garadkar
kmg_chem@unishivaji.ac.in

¹ Nanomaterials Research Laboratory, Department of Chemistry, Shivaji University, Kolhapur, Maharashtra 416004, India

² Material Science Laboratory, Department of Chemistry, Y. C. Warana Mahavidyalaya, Warananagar, Maharashtra 416113, India

³ Department of Physics, Shri. Vijaysinha Yadav Arts & Science College, Peth-Vadgaon, India

devices [17]. It is considered as the most promising semiconductor because of its unique optical, electronic and catalytic properties. Due to strong oxidizing power, high photochemical stability and non-toxic nature, SnO₂ has gained more attention in the field of photocatalysis [18]. Doping the SnO₂ matrix with the suitable rare earth metal ion could introduce defects which reduces the optical gap and hence enhances the photocatalytic activity [2].

In the present paper, biosynthesis of pure and Eu³⁺ doped SnO₂ nanoparticles prepared by microwave assisted sol–gel method using *Calotropis gigantea* (*C.G.*) leaf extract has been described. The different types of phytochemical constituents are flavonoids, terpenoids, triterpenoids, saponins, resins, protease, esters of calotropeoles polyphenolic compounds present in the *C.G.* as discussed in the previous reported paper [9] play important role in the synthesis of SnO₂ NPs. The plant has strong antioxidant property due to which for the synthesis of metal NPs the plant has become potential reducing and stabilizing agent [19]. The effect of the Eu³⁺ content on the photocatalytic properties of SnO₂ NPs in case of photodegradation of MO under UV-light illumination was investigated carefully.

2 Materials and methods

Tin (IV) chloride pentahydrate (SnCl₄·5H₂O) and europium nitrate pentahydrate (Eu (NO₃)₃·5H₂O) used in the present study were of analytical grade purchased from Sigma Aldrich. The *C.G.* leaves were collected from Kolhapur district (India). Millipore water was used for the preparation of all the solutions.

2.1 Synthesis of Eu doped SnO₂ NPs

The synthesis of Eu doped SnO₂ NPs was carried out by using aqueous leaf extract of *C.G.* The detailed procedure for the leaf extract preparation is reported in the previous paper [9]. For the synthesis of Eu doped SnO₂ NPs, 0.1 mol% of europium nitrate solution was added into 40 mL of stannic chloride solution (0.05 M) and stirred on a magnetic stirrer for thorough mixing of the solution. To this solution, appropriate quantity of aqueous leaf extract of *C.G.* was added dropwise with constant stirring. The gelatinous precipitate was obtained after complete addition of leaf extract. The supernatant solution was decanted and the as-obtained precipitate was washed with distilled water for several times and particles were separated by centrifugation. The precipitate was dried in the microwave oven at 900 W for 20 min (20 s on 40 s off cycle). Finally, the obtained dried powder was finely crushed in mortar and pestle, then crushed powder was kept for calcination at 400 °C up to 3 h.

2.2 Characterization

The XRD patterns of Eu doped SnO₂ NPs were obtained using a panalytical diffractometer [Model D2 PHASER]. Diffuse reflectance spectra of NPs were obtained using UV–Vis spectrophotometer (JASCO V-770). FT-IR spectra were obtained by using an FT-IR spectrophotometer (JASCO-4600, Japan). The shape and size of NPs were investigated by using transmission electron microscopy (JEM-2010, JEOL). The field emission-scanning electron microscopy (FE-SEM) and EDAX images were obtained using (JEOL-JSM-6360). Photoluminescence (PL) spectra were recorded on spectrofluorometer (FP-8200, JASCO, Japan). The dye concentration was measured by UV-Vis spectrophotometer (Shimadzu, Model UV-3600).

2.3 Photocatalytic degradation of methyl orange

The photocatalytic activities of synthesized Eu doped SnO₂ NPs were evaluated via degradation of MO dye ($\lambda_{\text{max}} = 464$ nm) solution at room temperature. In a typical photodegradation process, 0.15 g of photocatalyst was dispersed in 100 mL aqueous dye solution (20 ppm). The photocatalytic activity of SnO₂ NPs was tested at ambient condition under UV–visible light ($\lambda = 365$ nm) irradiation, which was obtained from high-pressure mercury lamp (Philips, HPL-N, 250W). The adsorption–desorption equilibrium was established by stirring the suspension in dark for 30 min prior to the irradiation. After irradiating the solution with UV-light, 3 mL suspension was withdrawn in the periodic time intervals of 30 min. Then the withdrawn solution was centrifuged and the supernatant solution was collected to determine absorbance of the dye solution by using spectrophotometer.

3 Results and discussion

3.1 X-ray diffraction patterns pure SnO₂ and Eu doped SnO₂ NPs

Figure 1 shows the X-ray diffraction (XRD) profiles for Eu doped SnO₂ NPs with Eu concentration from 0 to 0.125 mol%. The indexing of XRD peaks was carried out by using JCPDS Card No. 41-1445. All the observed peaks indexed to tetragonal rutile structure of SnO₂; there is no indication of Eu₂O₃ or Eu₂SnO₇ peaks; which confirmed the incorporation of the dopant into lattice site of SnO₂. By concentrating on the (211) peak for different Eu³⁺ dopant concentrations shown in Fig. 2, broadening and slight shifting of peaks towards higher angle than the pure SnO₂ is observed. This suggests that the

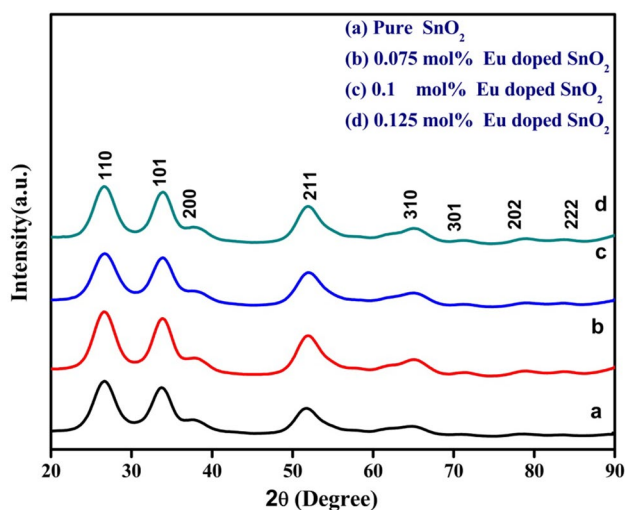


Fig. 1 XRD patterns of Eu³⁺ doped SnO₂ nanoparticles at different concentrations

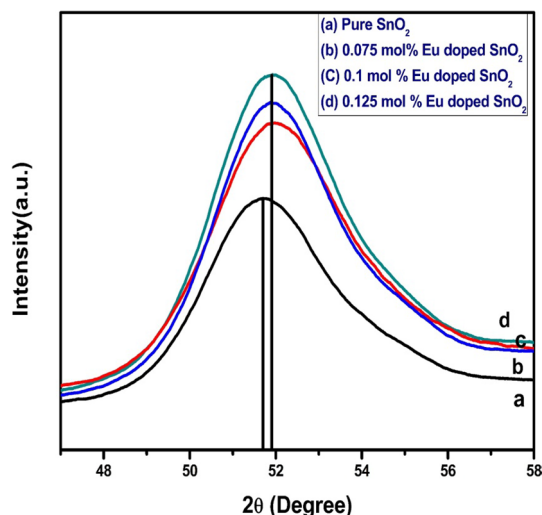


Fig. 2 XRD peak (211) shifting for Eu³⁺ doped SnO₂ nanoparticles at different concentrations

incorporation of Eu³⁺ into the SnO₂ lattice which leads to imperfection in crystals. This can be explained by Bragg’s law Eq. 1.

$$n\lambda = 2d \sin \theta \tag{1}$$

Table 1 Structural and Optical parameters of Eu³⁺ doped SnO₂ nanoparticles

Concentration of Eu dopant (mol%)	Bandgap energy (eV)	Crystallite size (nm)	Lattice constants (Å)		Microstrain (ε)
			a=b	c	
0.000	3.10	35	4.7220	3.1943	0.0124
0.075	3.08	28	4.7222	3.1955	0.0126
0.100	3.00	25	4.7251	3.1978	0.0127
0.125	3.30	24	4.7493	3.2000	0.0136

In the present case, after doping 2θ values are increases which indicates a decrease in the interplanar distance (d); that may cause by the fact that the ionic radius of Eu³⁺ (0.095 nm) is larger than that of Sn⁴⁺ (0.071 nm) [20]. From this fact, it is clear that with increase in dopant concentration, slight increase in the lattice parameters takes place. This indicates Eu³⁺ ions occupy the lattice sites of Sn⁴⁺ and leads to an increase in the interatomic distance and expansion in lattice parameters. The lattice constants of SnO₂ for a tetragonal structure where a = b ≠ c, were calculated by following Eq. 2.

$$\frac{1}{a^2} = \frac{h^2}{a^2} + \frac{k^2}{a^2} + \frac{l^2}{c^2} \tag{2}$$

Moreover, the average crystallite size corresponding to (110) peak was calculated by Scherrer’s formula. The crystallite size of SnO₂ decreases from 34 to 24 nm. The decrease in crystallite size (D) with increase in Eu concentration from 0.0 to 0.125 mol% observed, it indicates that the grain shrinkage due to Eu dopant is possible which leads to supersaturation. The grain shrinkage is induced by the surface segregation of the dopant ions on the surface, which can be stabilized by the progressive decrease of the surface energy and it can provide a barrier for the crystal growth diffusion [11, 21]. The broad XRD peaks of the sample obtained in the present condition are associated with crystallite size or microstrain or both. The presence of three types of imperfections like dislocation, stacking fault probability and lattice distortion in the SnO₂ crystal is responsible for the appearance of microstrain [22]. Microstrains are calculated by Eq. 3.

$$\epsilon = \frac{\beta \cos \theta}{4} \tag{3}$$

where β is the FWHM in radian, θ is the Bragg’s angle in degree. Microstrain of Eu doped SnO₂ NPs increased with increase in dopant concentration. The incorporation of the Eu³⁺ ions into the matrix could leads to larger mismatch. Therefore microstrain must be related to oxygen vacancies and site disorder [11]. The calculated crystallite size, lattice parameters, and microstrain are shown in Table 1 it is clear that with increase in Eu-doping concentration the crystallite size of SnO₂ NPs decreases and photocatalytic activity

increases. Also as crystallite size decreases, microstrain increases. Thus by doping of Eu in SnO₂ is responsible to increase in microstrain which ultimately enhances the photocatalytic activity.

3.2 FE-SEM and EDAX spectra of Eu doped SnO₂ NPs

The FE-SEM images of pure and 0.1 mol % Eu doped SnO₂ NPs are shown in Fig. 3a, b which show the agglomeration of the nanostructure in the 1 μm scale. Figure 4 shows the EDAX spectrum of Eu doped SnO₂ NPs which indicates the presence of O, Sn, and Eu in the NPs. The spectrum determines well-defined peaks at 0.5, 3.6, and 1.2, 5.7, 6.7, 7.7 keV relative to O, Sn and Eu respectively. The atomic % of Sn, O and Eu elements are 26.87, 53.2 and 0.18% respectively.

3.3 HR-TEM images of pure SnO₂ and Eu doped SnO₂ NPs

The HR-TEM images and SAED patterns of pure and Eu doped SnO₂ NPs are shown in Fig. 5. Figure 5a, d shows agglomeration in the SnO₂ and 0.1 mol% Eu doped SnO₂ NPs. Figure 5b, e shows the interplanar ‘d’ spacing calculated for (110) hkl planes of pure and 0.1 mol% Eu doped SnO₂ NPs. The SAED patterns of pure and 0.1 mol% Eu doped SnO₂ NPs are shown in Fig. 5c, f. The number of circular rings in SAED patterns indicates polycrystalline nature. In comparison with pure SnO₂, the circular rings of the Eu doped samples are dotted in nature indicating the small size of crystals.

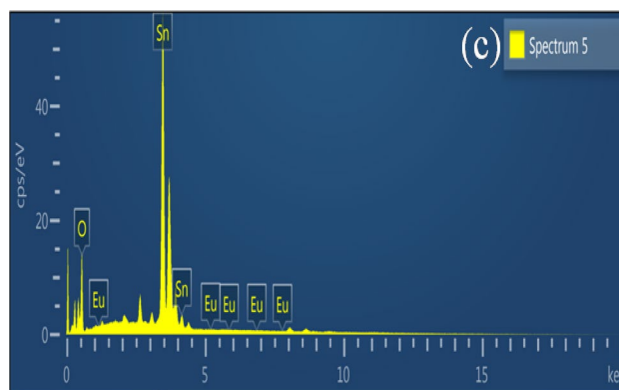


Fig. 4 EDAX spectrum of 0.1 mol% Eu³⁺ doped SnO₂ nanoparticles

3.4 UV–Vis diffuse reflectance spectra of SnO₂ NPs

The UV–Vis diffuse reflectance spectra of pure and Eu doped SnO₂ NPs in the range of 200–800 nm were scanned with varying concentration of Eu from 0 to 0.125 mol% as shown in Fig. 6. The Fig. 6. indicates a red shift in the absorption spectra due to Eu doping. It is clear that, as dopant concentration increased from 0 to 0.1 mol%, the absorption peak was shifted towards longer wavelength (red shift) as compared to the pure SnO₂ NPs. The optical bandgap of pure and Eu doped SnO₂ NPs with change in dopant concentration was obtained with the help of Tauc’s plot by extrapolating the $(\alpha h\nu)^2$ versus $h\nu$ as function of photon energy, as shown in Fig. 7. The band gap obtained are 3.1, 3.08 and 3.0 eV for pure SnO₂, 0.075 and 0.1 mol% Eu doped SnO₂ respectively. The decrease in bandgap with increase in dopant concentration may be due to the substitution of Eu³⁺ ions which introduced electron states into the bandgap of SnO₂ to form lowest unoccupied molecular orbital which intern increase

Fig. 3 FE-SEM images of a Pure SnO₂, b 0.1 mol% Eu³⁺ doped SnO₂ nanoparticles

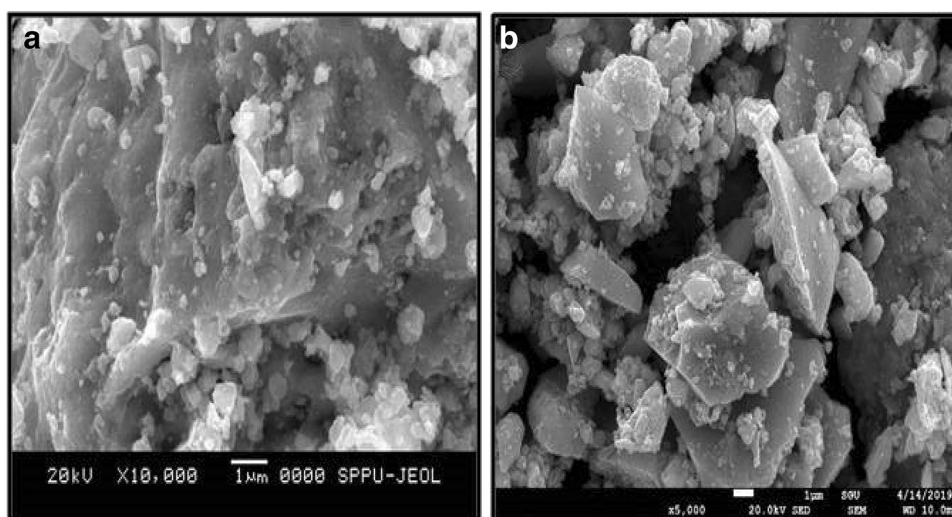


Fig. 5 **a** TEM image of pure SnO₂, **b** HR-TEM image of pure SnO₂, **c** SAED pattern of pure SnO₂, **d** TEM image of 0.1 mol% Eu³⁺ doped SnO₂, **e** HR-TEM images of 0.1 mol% Eu³⁺ doped SnO₂ and **f** SAED pattern of 0.1 mol% Eu³⁺ doped SnO₂

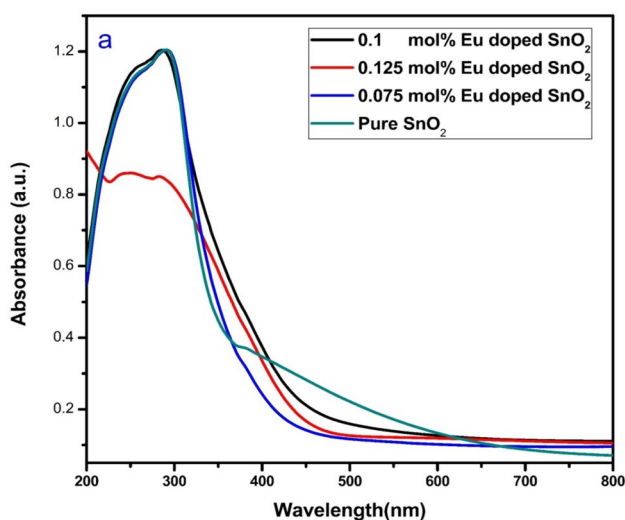
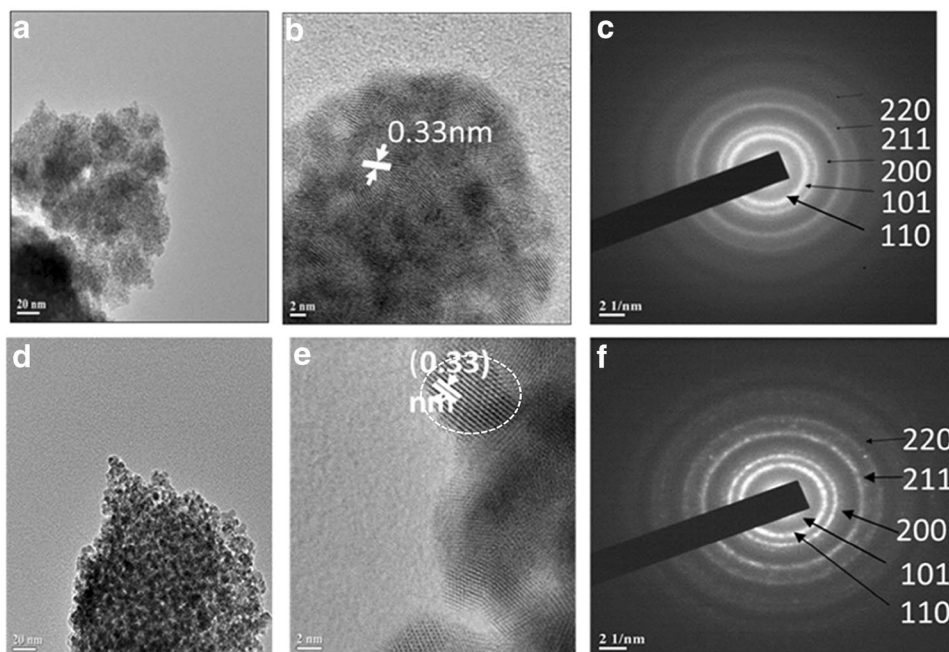


Fig. 6 UV-Vis diffuse reflectance spectra of Pure and Eu³⁺ doped SnO₂ nanoparticles at different concentration

the separation ratio of photoinduced electrons and holes and improves the photocatalytic activity of SnO₂ catalyst [23].

3.5 FT-IR spectra of pure SnO₂ and Eu doped SnO₂ NPs

The FT-IR spectrum of pure SnO₂ NPs shown in Fig. 8. The band at 3480 cm⁻¹ due to stretching vibrations of water molecule [24]. The absorbance peak at 2350 cm⁻¹ corresponds to C-H stretching and bending vibrations which shows presence of aldehydes, amines and aromatic ring.

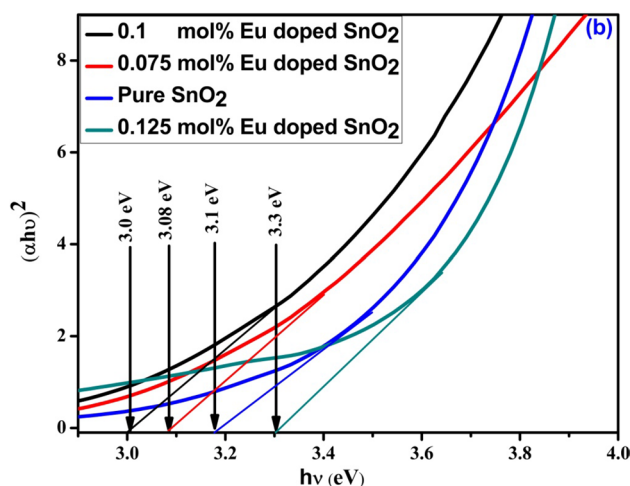


Fig. 7 Tauc plot for determination of bandgap of Pure and Eu³⁺ doped SnO₂ at different concentration

The peak at 620 cm⁻¹ is attributed to O–Sn–O bridge functional group of SnO₂ due to which the presence of SnO₂ in the crystalline phase is confirmed [25]. Figure 9 shows the FT-IR spectrum of 0.1 mol% Eu doped of SnO₂ NPs. The absorption peak at 3395 cm⁻¹ corresponds to the stretching vibration of O–H bond. Bending vibration of H–O–H bond from water molecule is responsible for peak at 1635 cm⁻¹. The OH as quencher of the Eu³⁺ ions emission will influence the energy transfer distance between the Eu and the host. The intense peak at 627 cm⁻¹ corresponds to stretching vibrations formed by the O–Sn–O bond. The appearance of unusual peak at 523 cm⁻¹ may be due to the defects on

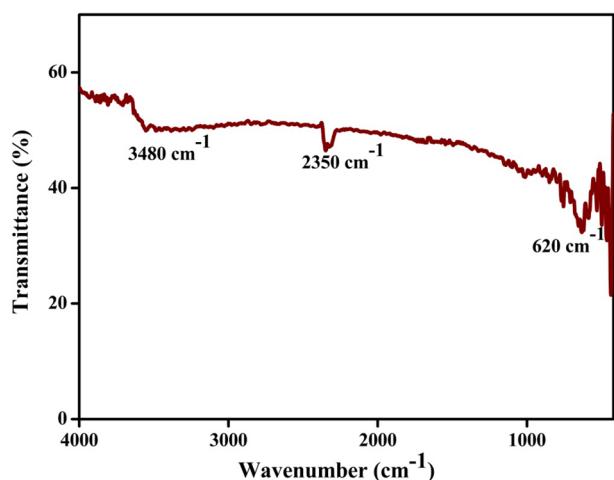


Fig. 8 FT-IR spectrum of Pure SnO₂ nanoparticles

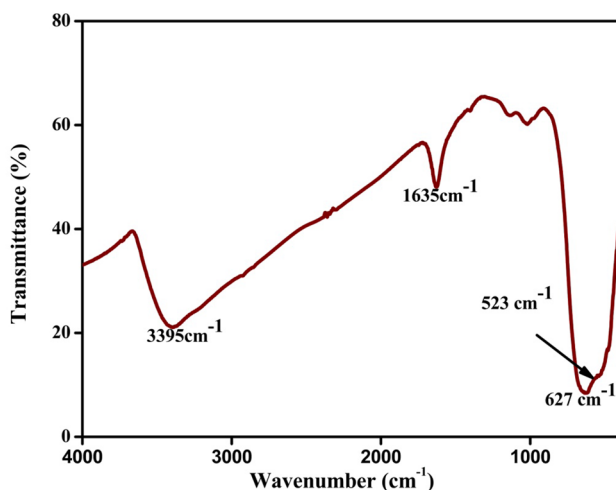


Fig. 9 FT-IR spectrum of 0.1 mol% Eu³⁺ doped SnO₂ nanoparticles

nanocrystalline surface because lattice dislocation would modify the local symmetry in the crystal, which allows the forbidden vibration mode to occur [26].

3.6 Photoluminescence (PL) spectra pure SnO₂ and Eu doped SnO₂ NPs

Figure 10 shows the PL spectra of Eu doped SnO₂ NPs with varying concentration ranging from 0.075–0.125 mol% at excitation wavelength 290 nm. The strongest ⁵D₀ → ⁷F₁ transition at 580 nm in Fig. 10 indicates high site symmetry, and Eu³⁺ ions are largely surrounded by SnO₂, however, no emission peak of Eu was observed. It is possible that weak Eu³⁺ ions emission peak was embedded in the signal from a strong, deep-level emission. From Fig. 10 it is clear that PL intensity decreases with increase in dopant concentration

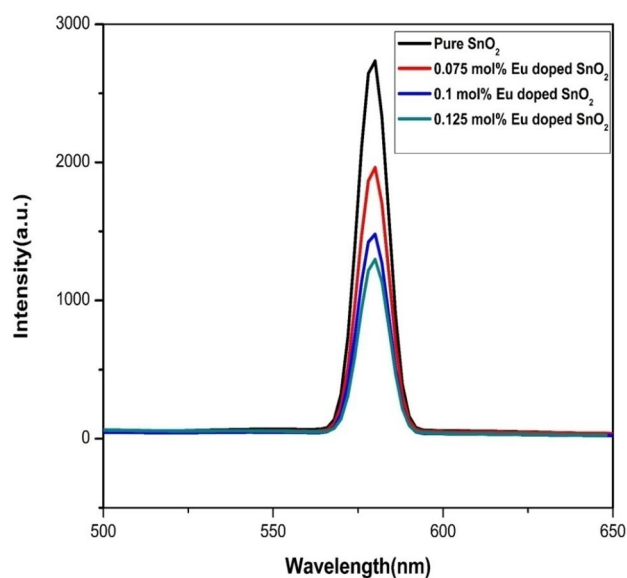


Fig. 10 Photoluminescence spectra of Eu³⁺ doped SnO₂ nanoparticles at different concentrations

and it can be attributed to concentration quenching effect which is described by cross relaxation process. The PL process involves exchange of energy between pair of neighboring ions and migration of excitation energy [27]. Doping the metal oxide with rare earth metal ion is responsible to increase number of surface defects which is responsible for the enhancement of photocatalytic activity, surface area and surface defects [28]. It is well known that the PL intensity is directly related to electron hole pair recombination rate. In general decrease in PL intensity leads to slow recombination rate so that it increases the life time of photogenerated charge carriers thereby enhancing the photocatalytic activity [29]. The results clearly indicates that in comparison with pure SnO₂, the Eu doped SnO₂ NPs shows significant quenching in PL intensity. This suggests that Eu doping is responsible to minimize the electron–hole pair recombination due to which better separation of photogenerated charge carriers takes place and hence there is enhancement in photocatalytic activity occurs.

3.7 Photocatalytic properties of Eu doped SnO₂ NPs

3.7.1 Effect of dopant concentration

The effect of dopant concentration on the photodegradation of MO dye under UV light is shown in Fig. 11. It can be seen that as the concentration of Eu in SnO₂ NPs increases from 0.075 to 0.1 mol%; the photodegradation rate of MO dye was also increased. However at 0.125 mol% of Eu concentration, sudden decrease in the photodegradation rate was observed. The enhancement in the photocatalytic activity is due to the

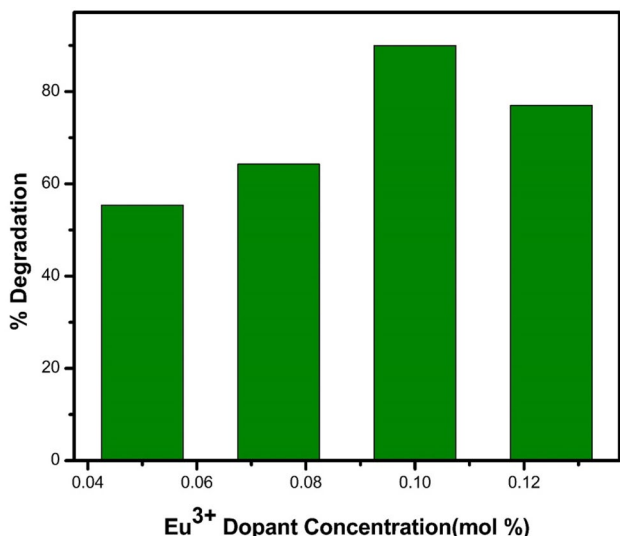


Fig. 11 Effect of Eu dopant concentration on photocatalytic degradation of MO

photogenerated electrons captured by suitable amount of dopant, which is responsible to decrease the rate of recombination of electron–hole. However, as the dopant concentration increases, the captured electron–hole pair starts to overcome the obstacles and recombine. On the other hand, the recombination becomes dominant, at certain concentration of dopant. The Eq. 4 shows that, at a certain dopant concentration, the rate of recombination exponentially increases with decrease in the distance between trap sites that’s why reduction in photocatalytic activity takes place [30].

$$K_{recomb} \propto \exp\left(\frac{-2R}{a_0}\right) \tag{4}$$

where, K_{recomb} is the rate of recombination, R is the distance between trap site of electron (e^-) and hole (h^+) and a_0 is the hydrogenic radius of wave function for charge carrier.

3.7.2 Plausible mechanism of photodegradation of Eu doped SnO₂ NPs

Along with the photocatalytic degradation experiments we have carried out several control experiments in order to ensure that the decrease in the dye concentration is due to the photocatalytic activity. The control experiments are (i) the adsorption of MO by Eu doped SnO₂ was checked by taking the photocatalyst into MO solution in the dark, the adsorption–desorption equilibrium was attained within 30 min and no significant change in concentration of MO was observed shown in Fig. 12a; (ii) the direct photolysis was carried out by irradiating the dye solution directly with the mercury lamp without photocatalyst, considerable change in concentration of

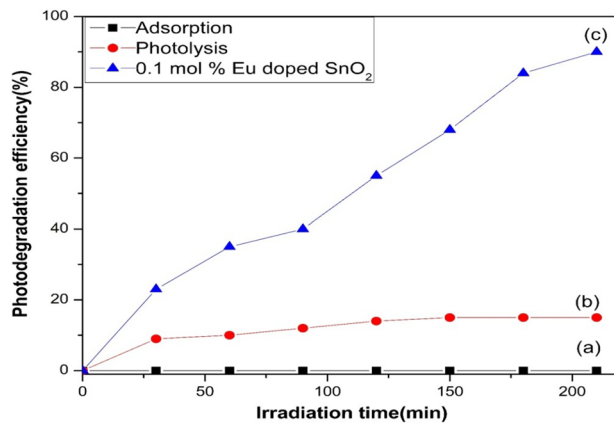


Fig. 12 Photodegradation of methyl orange (20 ppm) under UV light

the dye was observed shown in Fig. 12b The maximum degradation efficiency of 90% was observed by using 0.1 mol% Eu doped SnO₂ within 210 min shown in Fig. 12c.

The photocatalytic degradation of MO dye by using 0.1 mol% Eu doped SnO₂ NPs is shown in Fig. 13. The photodegradation of dye increases with increase in dopant concentration when irradiated under UV light ($\lambda = 365$ nm).

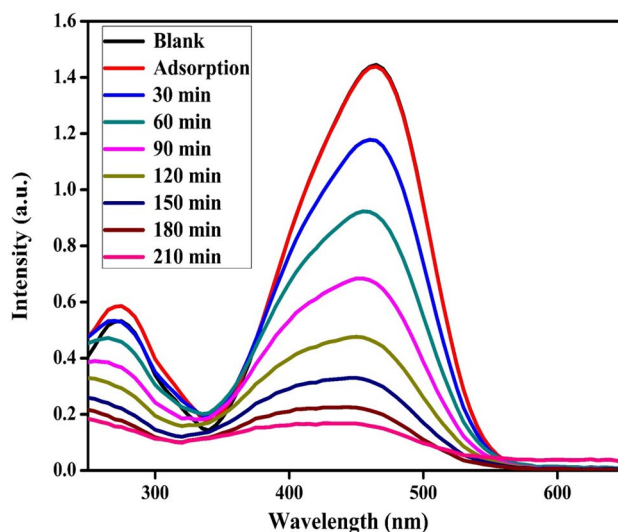
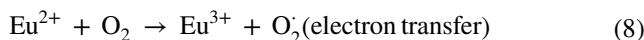
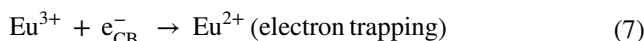
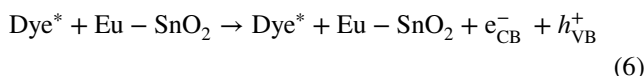
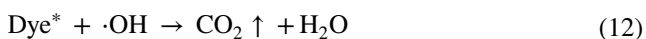
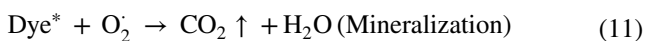
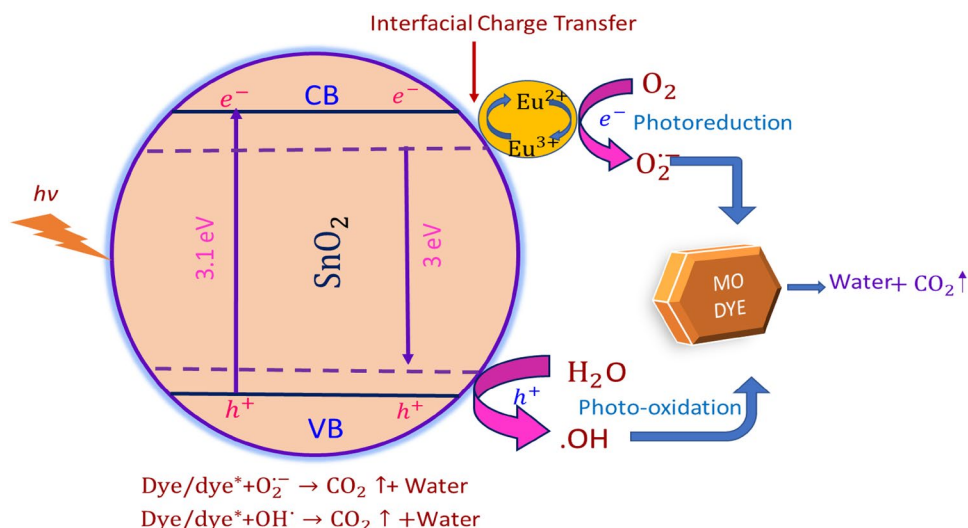


Fig. 13 Photocatalytic degradation of MO dye using 0.1 mol% Eu³⁺ doped SnO₂ nanoparticles

Fig. 14 Plausible photocatalytic degradation mechanism



The plausible mechanism for photocatalytic activity of Eu doped SnO_2 against MO dye is shown in Fig. 14 it is initiated by photoexcitation of the semiconductor, followed by the formation of electron–hole pairs (Eq. 6). The recombination of these electron hole pairs reduces the photocatalytic activity of SnO_2 NPs. Therefore Eu dopant is used along with SnO_2 NPs. The width of bandgap energy levels between valence band and conduction band get reduced due to introduction of Eu^{3+} in SnO_2 NPs. Being a p-type dopant, the Eu^{3+} ions act as electron scavenger and inhibit recombination rate resulting in an increase in photocatalytic activity [31]. Eu^{3+} ions are get reduced to Eu^{2+} by trapping the surface electrons (Eq. 7). The Eu^{2+} thus formed get readily oxidised back to Eu^{3+} by transferring the e^- to surface adsorbed oxygen as the standard reduction potential of $\text{Eu}^{3+}/\text{Eu}^{2+}$ is more electronegative (-0.43 eV) than the standard electrode potential of O_2/O_2^- (-0.33 eV) (Eq. 8). Eu doping enhances the oxygen availability on the surface of the catalyst as Eu being lanthanide ion have special electronic structure of $4f^x5d^y$ which would be able to form the labile oxygen species [32, 33].

The active OH^\cdot radicals generated by the transfer of charge from h_{VB}^+ to the H_2O molecule which is capturing the catalyst surface. The OH^\cdot and photogenerated h^+ are extremely strong, non-selective oxidant which leads to the partial or complete degradation of several organic chemicals on the catalysts surface [34]. The OH^\cdot radical being strong oxidising agent degrades the dye into CO_2 and water.

4 Conclusions

Eu doped SnO_2 NPs were prepared by environment friendly biosynthesis process using aqueous leaf extract of *C. G.* by microwave assisted sol gel technique. The synthesized Eu doped SnO_2 NPs were used for the photocatalytic degradation of MO dye. The dopant concentration has strong impact on the photocatalytic activity of the SnO_2 NPs. The optimum Eu^{3+} concentration in SnO_2 NPs was found to be 0.1 mol%, at which 90% photodegradation of MO dye was obtained. The effect of doping of appropriate ions into host lattice for the enhancement of photocatalytic activity can be attributed to increase in electron trapping owing to their higher surface sites and difference in bandgap energy.

Acknowledgements One of the authors KMG is gratefully acknowledges to Shivaji University, Kolhapur for providing research grant under Research Strengthening Scheme (File No. SU/BC U.D.Section/87/1385 Dated: 28/03/2019). We are also thankful to the SAIF-NEHU, Shillong for providing TEM facility.

References

1. J.C. Sin, S.M. Lam, I. Satoshi, K.T. Lee, A.R. Mohamed, Appl. Catal. B **148–149**, 258 (2014)
2. G.A. SuganyaJosephine, S. Ramachandran, A. Sivasamy, J. Saudi Chem. Soc. **19**, 549 (2015)
3. J. Singh, T. Dutta, K. Kim, M. Rawat, P. Samddar, P. Kumar, J. Nanobiotechnol. **16**, 1 (2018)
4. P. Kuppusamy, M.M. Yusoff, G.P. Maniam, N. Govindan, Saudi Pharma. J. **24**, 473 (2016)
5. R. Raliya, P. Biswas, J.C. Tarafdar, Biotechnol. Rep. **5**, 22 (2015)
6. G. Nabi, Q. Aain, N.R. Khalid, M.B. Tahir, M. Rafique, M. Rizwan, S. Hussain, T. Iqbal, A. Majid, J. Inorg. Organomet. **28**, 1552 (2018)

7. R. Rathnasamy, P. Thangasamy, R. Thangamuthu, S. Sampath, V. Alagan, *J. Mater. Sci.* **28**, 10374 (2017)
8. S.S. Hassan, W. Azab, H.R. Ali, M.S. Mansour, *Adv. Nat. Sci.* **6**, 1 (2015)
9. T.T. Bhosale, H.M. Shinde, N.L. Gavade, S.B. Babar, V.V. Gawade, S.R. Sabale, R.J. Kamble, B.S. Shirke, K.M. Garadkar, *J. Mater. Sci.* **29**, 6826 (2018)
10. D. Chandran, L.S. Nair, S. Balachandran, K.R. Babu, M. Deepa, *Bull. Mater. Sci.* **39**, 27 (2016)
11. Y. Zhao, Y. Li, X. Ren, F. Gao, H. Zhao, *Nanomaterials* **7**, 410 (2017)
12. A. Dieguez, A. Romano-Rodriguez, J.R. Morante, U. Weimar, M. Schweizer-Berberich, W. Gopel, *Sens. Actuators B.* **31**, 1 (1996)
13. A. Klein, C. Korber, A. Wachau, F. Sauberlich, Y. Gassenbauer, S.P. Harvey, D.E. Proffit, T.O. Mason, *Materials* **3**, 4892 (2010)
14. S.P. Kim, M.Y. Choi, H.C. Choi, *Mater. Res. Bull.* **74**, 85 (2016)
15. J. Yao, X. Shen, B. Wang, H. Liu, G. Wang, *Electrochem. Commun.* **11**, 1849 (2009)
16. S. Gubbala, V. Chakrapani, V. Kumar, M.K. Sunkara, *Adv. Funct. Mater.* **18**, 2411 (2008)
17. L.C. Nehru, V. Swaminathan, C. Sanjeeviraja, *Am. J. Mater. Sci.* **2**, 6 (2012)
18. L.P. Singh, M.N. Luwang, S.K. Srivastava, *New J. Chem.* **38**, 115 (2014)
19. M.I. Dina, A.G. Nabia, A. Rania, A. Aihetashamb, M. Mukhtarb, *ENMM* **9**, 29 (2018)
20. J. Sawahata, *Thin Solid Films* **656**, 1 (2018)
21. G. Wang, Y. Yang, Q. Mu, Y. Wang, *J. Alloys Compd.* **498**, 81 (2010)
22. S.V. Kite, D.J. Sathe, S.S. Patil, P.N. Bhosale, K.M. Garadkar, *Mater. Res. Express* **6**, 1 (2019)
23. S. Haya, O. Brahmia, O. Halimi, M. Sebais, B. Boudine, *Mater. Res. Express* **4**, 1 (2017)
24. S. Blessi, M.M.L. Sonia, S. Vijayalakshmi, S. Pauline, *Int. J. Chem. Tech. Res.* **6**, 2153 (2014)
25. N.M. Shaalan, D. Hamad, A.Y. Abdel Latief, M.A. Abdel-Rahim, *Prog. Nat. Sci.* **26**, 145 (2016)
26. J. Chen, J. Wang, F. Zhang, D. Yan, G. Zhang, R. Zhuo, P. Yan, *J. Phys. D* **41**, 1 (2008)
27. G. Singh, N. Kohli, R.C. Singh, *J. Mater. Sci.* **28**, 2257 (2017)
28. K. Yu, J. Shi, Z. Zhang, Y. Liang, W. Liu, *J. Nanomater.* **2013**, 1 (2013)
29. U. Alam, A. Khan, D. Ali, D. Bahnemann, M. Muneer, *RSC Adv.* **8**, 17582 (2018)
30. Y. Yang, X.J. Li, J.T. Chen, L.Y. Wang, *J. Photochem. Photobiol. A* **163**, 517 (2004)
31. N.U. Saqib, R. Adnan, I. Shah, *Environ. Sci. Pollut. Res.* **23**, 15941 (2016)
32. M. Mallanaicker, M. Mani, S. Nallasivam, R. Ariyamuthu, M. Velayutham, *RSC Adv.* **6**, 35024 (2016)
33. R. Kumar, A. Umar, G. Kumar, M.S. Akhtar, Y. Wange, S.H. Kim, *Ceram. Int.* **41**, 7773 (2015)
34. P.V. Korake, A.N. Kadam, K.M. Garadkar, *J. Rare Earths* **32**, 306 (2014)

Publisher's Note Springer Nature remains neutral with regard to jurisdictional claims in published maps and institutional affiliations.